

# STEP: Simultaneous Tracking and Estimation of Pose for Animals and Humans

Shashikant Verma<sup>1\*</sup>, Harish Katti<sup>2</sup>, Soumyaratna Debnath<sup>1</sup>, Yamuna Swami<sup>2</sup>,  
Shanmuganathan Raman<sup>1</sup>

<sup>1\*</sup>Department of Electrical Engineering, Indian Institute of Technology Gandhinagar,  
382355, Gujarat, India.

<sup>2</sup>National Institute of Mental Health, National Institutes of Health, MD 20892, Bethesda,  
USA.

\*Corresponding author(s). E-mail(s): [shashikant.verma@iitgn.ac.in](mailto:shashikant.verma@iitgn.ac.in);  
Contributing authors: [kattih2@nih.gov](mailto:kattih2@nih.gov); [debnathsoumyaratna@iitgn.ac.in](mailto:debnathsoumyaratna@iitgn.ac.in);  
[yamuna.narayanaswamy@nih.gov](mailto:yamuna.narayanaswamy@nih.gov); [shanmuga@iitgn.ac.in](mailto:shanmuga@iitgn.ac.in);

## Abstract

We introduce STEP, a novel framework utilizing Transformer-based discriminative model prediction for simultaneous tracking and estimation of pose across diverse animal species and humans. We are inspired by the fact that the human brain exploits spatiotemporal continuity and performs concurrent localization and pose estimation despite the specialization of brain areas for form and motion processing. Traditional discriminative models typically require predefined target states for determining model weights, a challenge we address through Gaussian Map Soft Prediction (GMSP) and Offset Map Regression Adapter (OMRA) Modules. These modules remove the necessity of keypoint target states as input, streamlining the process. Our method starts with a known target state initialized through a pre-trained detector or manual initialization in the initial frame of a given video sequence. It then seamlessly tracks the target and estimates keypoints of anatomical importance as output for subsequent frames. Unlike prevalent top-down pose estimation methods, our approach doesn't rely on per-frame target detections due to its tracking capability. This facilitates a significant advancement in inference efficiency and potential applications. We train and validate our approach on datasets encompassing diverse species. Our experiments demonstrate superior results compared to existing methods, opening doors to various applications, including but not limited to action recognition and behavioral analysis.

**Keywords:** Pose Estimation, Visual Tracking, Target Model Prediction.

## 1 Introduction

Pose estimation is a fundamental and demanding task in computer vision, with diverse practical applications in the real world. When applied to video sequences, pose estimation proves invaluable across various uses, including but not limited to

action recognition, behavioral analysis, robotics, and surveillance, demonstrating its wide-ranging utility. Analyzing poses across videos involves tackling specific challenges, such as object detection, precise frame-to-frame tracking, and anatomical keypoint localization.

**Motivation.** Traditional top-down Pose Estimation Techniques require precise bounding box data, sourced either from automated detectors or manually annotated ground truths, to appropriately crop, center, and scale the images of the targets. These methods are designed with specific cropping standards that reflect established priors regarding the target shapes. Although these methods have been effective, their performance can diminish when encountering targets with non-standard aspect ratios, leading to less accurate pose estimation. To this end, we propose a transformer-based method to simultaneously handle tracking and pose estimation for the object within a video by concurrently estimating weights for three tasks: localization, tracking, and pose estimation. Integrating tracking eliminates the need for per-frame object detections used in existing top-down methods. Unlike these conventional approaches, our proposed method offers a robust alternative not hindered by variations in aspect ratios, enhancing its utility across diverse imaging conditions and target configurations.

**Pose Estimation.** Pose estimation approaches can be categorized into two main paradigms: top-down and bottom-up. The top-down approaches [Xu et al. \(2022\)](#) [Sun et al. \(2019\)](#) first detect the object of interest employing object detectors and subsequently conduct pose estimation for each detection. In contrast, the bottom-up approaches [Pishchulin et al. \(2016\)](#) [Ye et al. \(2023\)](#) [Insafutdinov et al. \(2016\)](#) directly regress the keypoints and later concentrate on associating the detected keypoints to the object. The top-down approach achieves accuracy at a higher cost with an extra detection step, while the bottom-up paradigm, though more efficient, attains lower accuracy. Traditional top-down Pose Estimation Techniques require precise bounding box data typically, a  $1.33$  height-to-width ratio for human subjects to accommodate their vertical orientation and a  $1.33$  width-to-height ratio for animals to capture their broader horizontal spread. CNN-based models used for regressing keypoints in pose estimation, like [Toshev and Szegedy \(2014\)](#) [Wei et al. \(2016\)](#) [Xiao et al. \(2018\)](#), face challenges in capturing image-specific dependencies because of static convolutional kernels. Furthermore, these models excel in revealing class-specific saliency maps rather than at establishing relationships between structural elements, such as the connection between anatomical

structure and keypoint locations within the pose context [Yang et al. \(2021\)](#).

**Visual Object Tracking.** Deep neural networks have shown remarkable performance in object tracking and pose estimation tasks. Within the tracking domain, two predominant methodologies have emerged: Siamese networks [Li et al. \(2018\)](#) and networks integrating discriminative appearance modules [Bhat et al. \(2019\)](#). Object Tracking deals with accurately identifying and tracking each target object within video streams. This field has progressed significantly due to advances in object detection technologies, with most modern trackers adopting the tracking-by-detection approach. This technique applies an object detector across successive frames to generate detections that are then used for tracking. Centernet [Duan et al. \(2019\)](#) is commonly employed in many tracking-by-detection systems due to its operational efficiency, whereas YOLOX [Ge et al. \(2021\)](#) has gained popularity for its exceptional detection accuracy. Typically, these methods incorporate the Kalman filter [Welch et al. \(1995\)](#) as a motion model to predict future tracklet positions. The Intersection over Union (IoU) metric is used to gauge the similarity between predicted and detected boxes for a reliable association. However, the Kalman filter is noted for its vulnerabilities, such as susceptibility to state noise and amplification of temporal discrepancies. Furthermore, the application of the Kalman filter, despite its widespread use, requires careful tuning of its parameters to mitigate the effects of its inherent vulnerabilities. To address these issues, some tracking systems have begun integrating more sophisticated deep learning-based motion models, which can offer improved robustness and accuracy in dynamic environments.

**Contribution.** Existing top-down approaches utilize object detectors like [Jiang et al. \(2022\)](#) [Li et al. \(2022\)](#) to determine a bounding box around the object for pose estimation. Object detectors primarily focus on recognizing and localizing objects within individual images rather than maintaining a (tracking) identity across frames, creating a gap in pose analysis within video sequences. Our proposed approach addresses this gap through tracking capability while simultaneously estimating pose keypoints. Our approach uses a transformer-based method to simultaneously handle tracking and pose estimation for the object within a video by concurrently estimating weights for three tasks:

localization, tracking, and pose estimation. Integrating tracking eliminates the need for per-frame object detections used in existing top-down methods. In summary, our contributions are as given below.

- We conduct a comprehensive study on the pose estimation task within a discriminative model prediction framework. We utilize a Transformer-based model prediction module while simultaneously tracking the object of interest—an unexplored area in previous research.
- We introduce the Gaussian Map Soft Prediction (GMSP) and Offset Map Regression Adapter (OMRA) modules, which work together to accurately localize key points corresponding to the target state, ensuring both efficiency and precision in pose key point estimation.
- In the inference phase, we propose a confidence-based memory update of our tracker. This update integrates previous frame outputs to supervise and estimate subsequent outputs effectively. We showcase the effectiveness of our approach through a case study on Awaji Monkey Center (AMC) video streams.

We begin by reviewing relevant works on tracking and pose estimation closely related to ours in Section 2. Following that, Section 3 provides a detailed explanation of our proposed methodology, including the network architecture and the steps involved in training STEP and performing inference. We demonstrate that our approach delivers competitive performance in pose estimation compared to state-of-the-art methods while also incorporating tracking. Notably, our method surpasses these approaches in top-down evaluations. Finally, Section 4 presents experiments and exhaustive ablation studies to validate our findings further.

## 2 Related Works

Our proposed approach is inspired by established discriminative model prediction paradigms used in visual object tracking [Bhat et al. \(2019\)](#) [Danelljan et al. \(2019\)](#) [Dai et al. \(2019\)](#) [Mayer et al. \(2022\)](#). We explore the potential of this framework to predict keypoints for pose estimation while performing tracking simultaneously. In contrast to prevailing trends, which often focus on solving dedicated tasks sequentially, we demonstrate

how vision transformer-based discriminative model weight predictions bridge the gap, enabling simultaneous predictions instead of sequential estimations. Vision Transformers have demonstrated significant promise across various other related vision tasks, such as Recognition [Dosovitskiy et al. \(2020\)](#), Object Detection [Carion et al. \(2020\)](#), and Segmentation [Strudel et al. \(2021\)](#). Recently, numerous studies have explored the potential of Vision Transformers for tracking [Chen et al. \(2021\)](#) and Pose estimation [Xu et al. \(2022\)](#) [Yang et al. \(2021\)](#). The discriminative features predicted by transformers for bounding box regression in tracking have demonstrated more promising outcomes than predictions from traditional optimization-based discriminative models. Additionally, in pose estimation, the transformer architecture [Vaswani et al. \(2017\)](#) holds a distinct advantage over CNNs due to its attention layers, facilitating the model in capturing interactions among any pair of keypoint locations. We now present an overview of existing literature emphasizing Transformers within the domains of pose estimation and tracking tasks on video sequences.

### 2.1 Vision Transformers for Tracking

Modern trackers such as [Carion et al. \(2020\)](#) [Chen et al. \(2021\)](#) [Yu et al. \(2021a\)](#) utilize transformers to predict discriminative features for target localization and bounding box regression. These trackers involve a transformer encoder that encodes target-related features, followed by a transformer decoder that combines training and test features using cross-attention layers to compute discriminative features [Wang et al. \(2021\)](#) [Yu et al. \(2021a\)](#) [Chen et al. \(2021\)](#). Two specialized modules are employed by [Yu et al. \(2021a\)](#) for tasks of localization and bounding box regression, while [Chen et al. \(2021\)](#) utilizes a feature fusion module. In [Zhang et al. \(2021\)](#), a Multi-object tracker (MOT) is introduced, drawing inspiration from tracking by detection. Additional works sharing a similar approach, such as [Danelljan et al. \(2019\)](#) [Bhat et al. \(2019\)](#), incorporate a memory state to update online trackers. Expanding on the transformer architecture introduced in [Carion et al. \(2020\)](#) [Mayer et al. \(2022\)](#) [Mayer et al. \(2024\)](#) presents a transformer-based model predictor that estimates weights for localization and bounding box regression tasks.

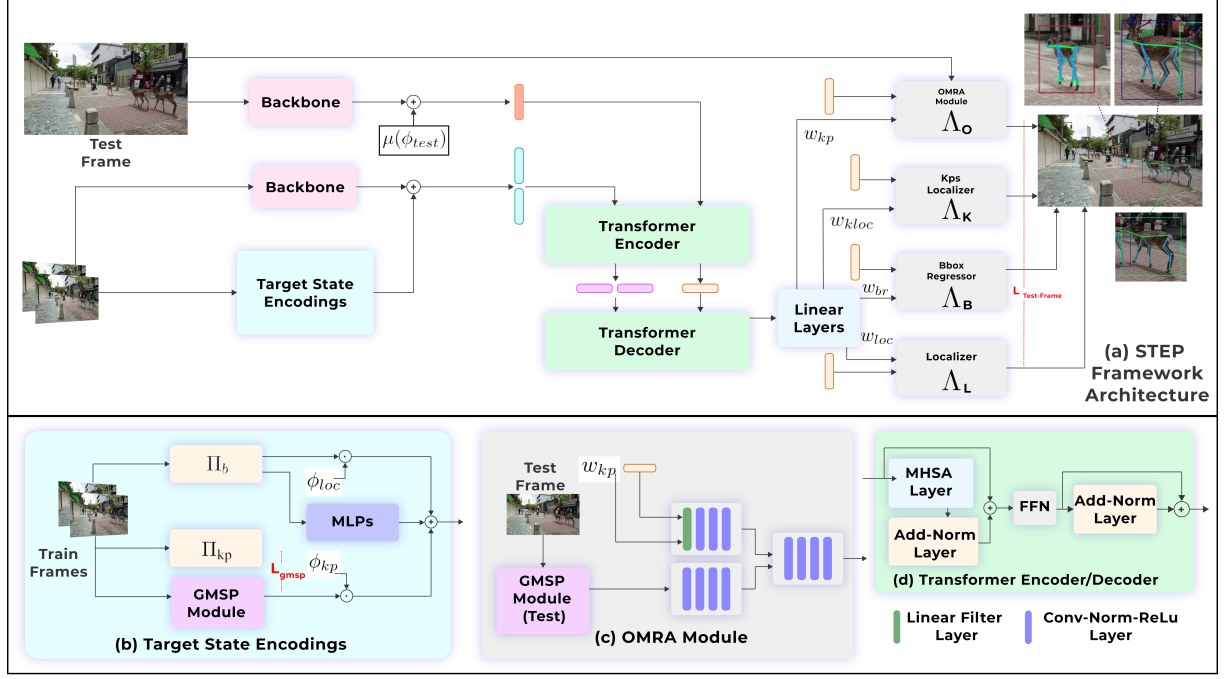


**Fig. 1** The proposed STEP framework for simultaneous tracking and pose estimation. (a) the full architecture, (b) the calculation of Target State Encodings, (c) the architecture of the offset map regression adapter (OMRA) module, and (e) the standard transformer architecture comprising multi-headed self-attention blocks.

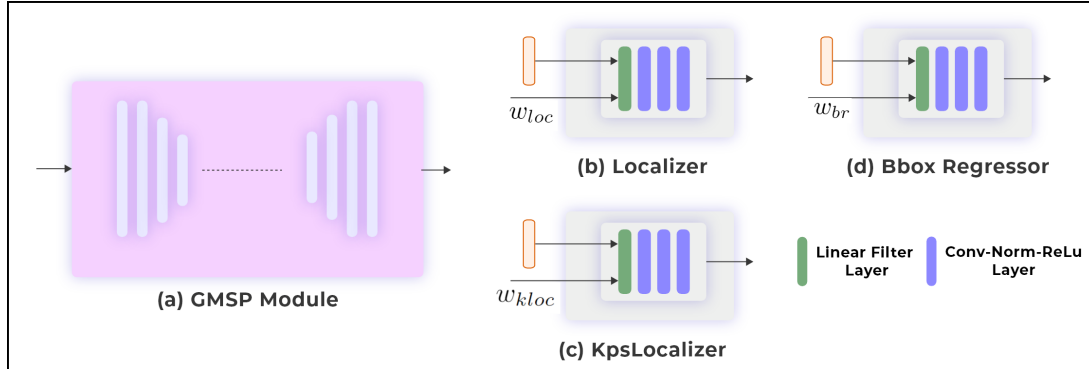


**Fig. 2** Modules of STEP architecture are shown (a) GMSP Module, (b) Localizer Module  $\Lambda_L$ , (c) Keypoint Localizer Module  $\Lambda_K$ , and (d) Bounding Box Regressor Module  $\Lambda_B$ .

## 2.2 Vision Transformers for Pose Estimation

The evolution of pose estimation methods has swiftly transitioned from CNNs [Xiao et al. \(2018\)](#) to vision transformer-based networks due to their robust feature representation capabilities. In contrast to how transformers are used in discriminative model prediction-based tracking approaches, studies in pose estimation view transformers as more

effective decoders [Li et al. \(2021a\)](#) [Li et al. \(2021b\)](#) [Li et al. \(2024\)](#). In [Yang et al. \(2021\)](#), the transformer architecture processes feature to capture global relationships within images. Introducing a token-based representation, [Li et al. \(2021b\)](#) models relationships among pose keypoints. Additionally, HRFormer [Yuan et al. \(2021\)](#) utilizes transformers to learn high-resolution features.



These transformer-based pose estimation methods outperform widely used keypoint estimation benchmarks compared to CNN-based methods. Investigating the capabilities of straightforward vision transformers, Xu et al. (2022) explores simplified transformer baselines, eliminating heavy-weight CNN-based feature extractors or intricate transformer architectures present in existing neural models. More recently, pose estimation in challenging scenarios, such as low-light images and limited annotations, has been addressed in Ai et al. (2024) and Li and Lee (2023).

### 2.3 Pose Estimation and Tracking in videos

Object tracking and pose estimation in videos have extensive applications, including action recognition Bouchrika et al. (2011) and the analysis of human or animal behavior in various environments. Notably, markerless pose estimation is gaining popularity in neuroscience and the study of animal behaviors Coria-Avila et al. (2022). Expanding on the widely used CNN-based architecture of the DeepLabCut model Mathis et al. (2018), Lauer et al. (2022) extends it to facilitate multi-animal tracking and pose estimation. SLEAP Pereira et al. (2022) employs a lightweight CNN, effectively tracking insects (drosophila, bees) and rodents. In these approaches, pose estimation occurs frame-by-frame, while the tracking framework relies on a computationally intensive optical flow-based method. An encoder-decoder setup is proposed by Sun et al. (2022) to encode input frames and train the model for reconstructing spatiotemporal differences between video frames for keypoint discovery. Several studies have concentrated on analyzing human poses across videos. Approaches such as Xiao et al. (2018) Yang et al. (2021) Yuan et al. (2021) involve framewise detections followed by dedicated modules for identification across frames.

## 3 Methodology

This work introduces STEP, a Transformer-based target model prediction network that conducts simultaneous tracking and pose estimation by predicting keypoints. We first provide a concise overview of existing Optimization and Transformer-based model predictors and then elaborate on our proposed approach, STEP, outlining its network

architecture, training, and inference procedures in detail.

### 3.1 Background

Existing discriminative models like Bhat et al. (2019) Danelljan et al. (2019) Dai et al. (2019) Zheng et al. (2020) typically adhere to a shared foundational framework. They aim to solve optimization problems, as presented in Equation 1, where the target model  $\mathcal{T}(\cdot)$  generates the intended target states.

$$w = \arg \min_{\hat{w}} \sum_{(x,y) \in \mathcal{S}_{train}} \phi(\mathcal{T}(\hat{w}; x), y) + \lambda r(\hat{w}) \quad (1)$$

Given a collection of training samples comprising a total of  $m$  training frames, denoted as  $\mathcal{S}_{train} = \{(x_i, y_i)\}_{i=1}^m$ , where  $x_i \in \mathcal{X}$  represents the high-dimensional feature map of the  $i$ -th frame and  $y_i \in \mathcal{Y}$  represents the corresponding desired target state. The optimization problem outlined in Equation 1 aims to attain the optimal weight  $w$  for the target model  $\mathcal{T}$ . This is achieved by minimizing residuals computed by the function  $\phi(\cdot)$ , which measures the error between the output of the target model and the ground truth labels  $y$ .  $r(\cdot)$  is a regularization term weighted by a scalar  $\lambda$ . Approaches following this optimization strategy optimize weights with limited information, relying solely on the provided training frames. Furthermore, they struggle to incorporate learned priors into the target model. Rather than directly minimizing the objective outlined in Equation 1, Mayer et al. (2022) introduces a Transformer-based model predictor approach. This method predicts target model weights solely from data through end-to-end learning. Nevertheless, their primary emphasis lies in learning features that effectively differentiate the target state from previously encountered states within  $\mathcal{S}_{train}$ . For pose estimation, the model predictor should precisely capture crucial information relevant to anatomical keypoints rather than solely concentrating on localization tasks.

### 3.2 Network Architecture

Our proposed network adopts an end-to-end learning approach to predict the weights of the target model purely from data. The overview of our methodology is depicted in Figure 1. We leverage a baseline network pre-trained on Imagenet Deng

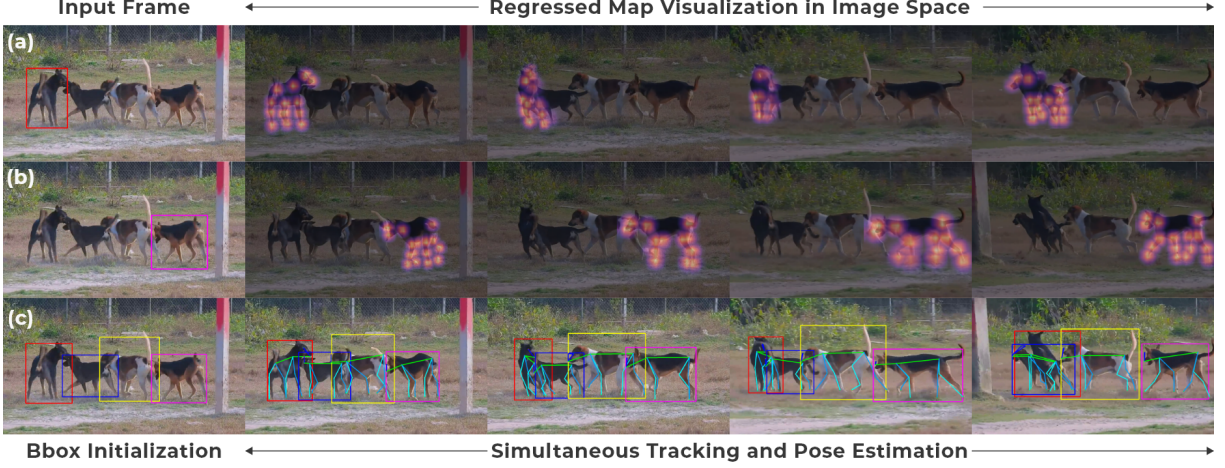


**Fig. 3** For a video sequence, columns display target score maps  $\hat{K}_{\text{gm}}$  when initiated with bounding boxes, as depicted in (a) and (b). In (c), our STEP framework runs concurrently for each bounding box to track and estimate the pose of respective targets. Notably, observe the robustness of STEP in estimating keypoints, particularly in scenarios involving occlusion. A failure case is showcased in the last frame of (c) for the red bounded target, stemming from ambiguous activations within the red target’s score map, as evident in the last frame of (a). Additional qualitative results across various species are provided in the Supplementary material.

et al. (2009) to extract high-dimensional image features. We closely adhere to the discriminative model prediction approach introduced by Mayer et al. (2022) and expand it to learn target model weights specifically for the keypoint regression task. Our rationale is rooted in the belief that this discriminative model prediction approach captures more target-specific information, making it suitable for distinguishing keypoints of anatomical importance. Unlike Mayer et al. (2022), our target state information includes information on  $k$ -keypoints crucial for the pose estimation task. The main components of our network are now described in detail.

### 3.2.1 Target State Encodings

Adhering to the established principles outlined in Xu et al. (2020) for precise tracking, tracking methodologies typically divide the task into two sub-tasks: localization and bounding box regression. Building upon this widely adopted approach, it becomes imperative to incorporate an additional step in our simultaneous pose estimation methodology, which involves deriving regression targets for estimating keypoint locations. Consider  $K^t \in \mathbb{R}^{2 \times k}$  as the ground truth representation of keypoints for the target object, comprising  $k$  keypoints, each denoted by  $K_i^t = (x_i, y_i)$ . Here,  $(x_i, y_i)$  represents

the coordinates of the  $i$ -th keypoint. We use the subscript  $t$  to highlight that the keypoints belong to the target object among the multiple object annotations present in the frames. Given a training frame  $I \in \mathbb{R}^{H_i \times W_i \times 3}$ , the pre-trained backbone network extracts its features  $X \in \mathbb{R}^{H_f \times W_f \times n}$  in  $n$ -dimensional space, scaling down the image space by factor  $s$ . We represent  $K_i^t$  at each pixel location  $(j^x, j^y)$  on the feature map  $X$  as follows,

$$\kappa_i = \left( \left\lfloor \frac{s}{2} \right\rfloor + s \cdot j^x - x_i, \left\lfloor \frac{s}{2} \right\rfloor + s \cdot j^y - y_i \right) \quad (2)$$

where  $H_i = s \cdot H_f$  and  $W_i = s \cdot W_f$ . This representation of keypoint  $K^t$  is denoted as offset map  $K_{\text{om}}^t = (\kappa_i)_{i=1}^k$  with  $K_{\text{om}}^t \in \mathbb{R}^{H_f \times W_f \times 2k}$ . Additionally, apart from the keypoint offset map  $K_{\text{om}}^t$  of the target, we generate a  $k$ -channel Gaussian map  $K_{\text{gm}}^t \in \mathbb{R}^{H_f \times W_f \times k}$ , where each channel  $i$  is a Gaussian map centered at the coordinate location of the  $i$ -th keypoint for all possible objects annotated in ground-truth. We create  $K_{\text{gm}}^t$  by retaining the Gaussian map for keypoints related to the object of interest (target object) and set all other Gaussian maps to zero. Adopting the widely recognized LTRB representation used in Mayer et al. (2022) Yu et al. (2021a), a bounding box  $\beta = \{b_{x_1}, b_{y_1}, b_{x_2}, b_{y_2}\}$  in  $xyxy$  format can be translated into the offset map  $B_{\text{om}} = \{\lfloor (s/2) \rfloor + s \cdot j^x -$

$b\} \forall b \in \beta$ . This  $B_{\text{om}} \in \mathbb{R}^{H_f \times W_f \times 4}$  is the offset map representation of the bounding box  $\beta$ . Moreover, we generate a Gaussian map  $B_{\text{gm}}$  centered at the center of the bounding box  $\beta$ , specifically for learning the localization task. In Figure 1(b), this estimation is illustrated by  $\Pi_b$  and  $\Pi_{kp}$  blocks. These maps,  $K_{\text{om}}^t, K_{\text{gm}}^t, K_{\text{gmsp}}, B_{\text{om}}$ , and  $B_{\text{gm}}$  act as regression targets for the localizer and regression modules, described in Section 3.3.

We utilize two learnable embeddings in  $n$  dimensions:  $\phi_{\text{loc}} \in \mathbb{R}^{1 \times n}$  and  $\phi_{\text{kp}} \in \mathbb{R}^{k \times n}$ . These embeddings are employed to distinguish between foreground and background information concerning target centers and keypoints, where  $k$  represents the number of keypoints. For a given training frame  $i$ , we combine the extracted deep features  $X$  with this target state information to create the training features for the Transformer module, as denoted in Equation 3.

$$f_i = X + \Psi_b(B_{\text{om}}) + \Psi_{\text{kp}}(K_{\text{om}}^t) + \phi_{\text{loc}} \cdot B_{\text{gm}} + \phi_{\text{kp}} \cdot K_{\text{gm}}^t \quad (3)$$

Here,  $\Psi$  denotes a neural network containing multiple Multilayer Perceptrons (MLPs) designed to map the offsets into higher dimensions with  $n$  channels, while the  $\cdot$  operation signifies element-wise multiplication. Equation 3's target states rely on  $K_{\text{om}}$  and  $K_{\text{gm}}$ , necessitating initialization with keypoint data. We propose GMSP and OMRA Modules to eliminate this dependency (Section 3.2.3). Assuming our GMSP module infers enriched information approximating Gaussian maps  $K_{\text{gmsp}}$ , we adjust Equation 3 as follows:

$$f_i = X + \Psi_b(B_{\text{om}}) + \phi_{\text{loc}} \cdot B_{\text{gm}} + \phi_{\text{kp}} \cdot K_{\text{gmsp}} \quad (4)$$

Moreover, we incorporate the test frame encoding, composed of deep features  $X_{\text{test}}$  and a learnable token  $\phi_{\text{test}}$ , resulting in  $f_{\text{test}} = X_{\text{test}} + \mu(\phi_{\text{test}})$ . Here,  $\phi_{\text{test}}$  represents the learnable token, and  $\mu(\cdot)$  signifies the repetition of the token for each dimension of  $X_{\text{test}}$ .

### 3.2.2 Transformer Encoder and Decoder

The transformer encoder and decoder utilize training features  $f_i$ , and test features  $f_{\text{test}}$  as inputs. It predicts the target model weights for target and keypoint localization ( $w_{\text{loc}}$  and  $w_{\text{kloc}}$ , respectively), along with weights for bounding box and

keypoint regression ( $w_{\text{br}}$  and  $w_{\text{kp}}$ , respectively). The transformer architecture, inspired by Yan et al. (2021), comprises multiple multi-headed self-attention modules Vaswani et al. (2017), as illustrated in Figure 1(d). Denoting the encoded versions of  $f_{\text{test}}$  and  $f_i$  as  $z_{\text{test}}$  and  $z_i$ , respectively, the regression modules take encoded test features as input, along with the target model weights, to predict the final outputs.

### 3.2.3 Regression Modules

We design the STEP framework to rely solely on the initial bounding box for input dependency. To maintain independence from initial keypoint-related inputs, we introduce the Offset Map Regression Adapter (OMRA) and Gaussian Map Soft Prediction (GMSP) module to incorporate target keypoint embeddings. This allows for simultaneous tracking and pose estimation for the target. We describe each module in detail below:

- **GMSP Module.** We utilize a straightforward encoder-decoder architecture, as shown in Figure 2 within the GMSP Module, to learn a soft map relevant to anatomically crucial keypoints of the target. This architecture involves several convolutional and deconvolutional blocks. More specifically, in our experiments, we use **two** convolutional blocks and **two** deconvolution blocks for the GMSP Module. As illustrated in Figure 1(b), we train the GMSP module exclusively on training frames, using  $\Pi_{kp}$  as supervision to predict a soft map of all possible key points within these frames. This training is performed solely on the training frames, ensuring that the GMSP module is not exposed to test-frame data during the encoding determination process. Given the training features  $f_i$  encoded with the state encoding of the target state bounding box  $\Pi_b$ , as defined in Equation 4, the transformer predicts model weights  $w_{\text{kp}}$ , which are aware of the target state for the object being tracked. Finally, the adapter module, described below, follows a two-tower architecture to reason the final key points specific to the object of interest.
- **Offset Map Regression Adapter Module.** For training frames, the GMSP Module provides information relevant to target state keypoint information to estimate the training feature  $f_i$ . GMSP collaborates with the OMRA Module for

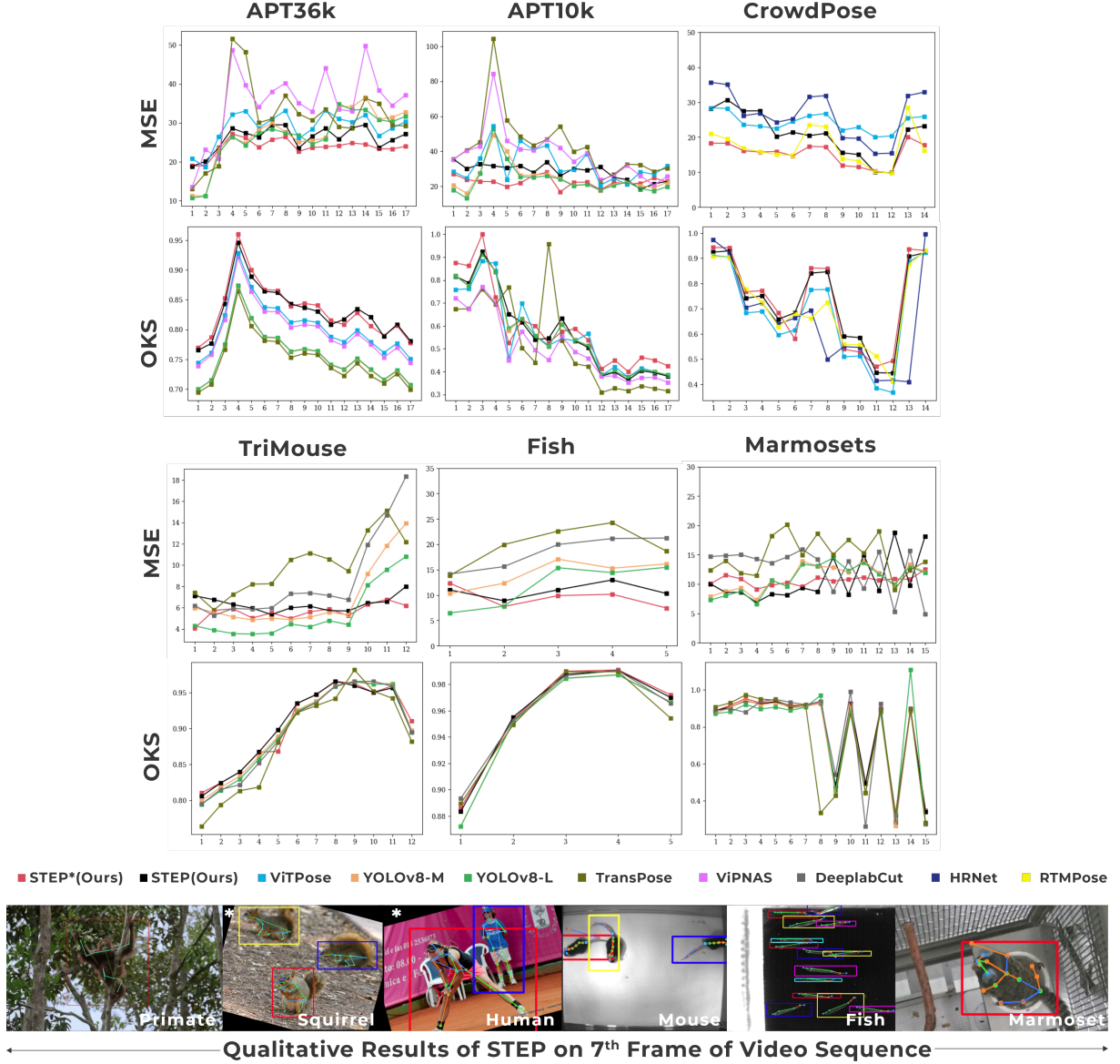


**Fig. 4** Comparison of Mean Squared Error (MSE) and Object Keypoint Similarity (OKS) for individual keypoints against various existing methods: ViTPose [Xu et al. \(2022\)](#), YOLOv8 [Jocher et al. \(2023\)](#), TransPose [Yang et al. \(2021\)](#), ViPNAS [Xu et al. \(2021\)](#), DeepLabCut [Lauer et al. \(2022\)](#), HRNet [Sun et al. \(2019\)](#), and RTMPose [Jiang et al. \(2023\)](#). Notably, the marmoset dataset features top-view images of marmosets in a cage with infrequent occurrences of lower limb keypoints. The inherent imbalance in training data leads to notable inaccuracies across all methods for the four bottom-limb keypoints. Moreover, the bottom row displays the output of our approach on a frame from the corresponding dataset’s video sequence, where \*-marked frames are from synthetic sequences.

the test frame through a two-tower-based architecture, as illustrated in Figure 1(c). In line with [Yan et al. \(2021\)](#), the first tower computes an attention map using the target model weights  $w_{kp}$ , expressed as  $w_{kp} * z_{test}$ . The second tower handles the output from the GMSP Module.

The outputs from both towers are fused using a concatenation operation and then further processed with a CNN. The first tower comprises an attention computation layer followed by **three** Conv-Norm-ReLU layers. The second tower processes soft predictions from the GMSP Module



**Table 1** Comparison with state-of-the-art methods for pose estimation, including TransPose Yang et al. (2021), YOLO-v8 Jocher et al. (2023), ViPNAS Xu et al. (2021), ViTPose Xu et al. (2022), DeepLabCut Lauer et al. (2022), RTMPose Jiang et al. (2023), and HRNet Sun et al. (2019). We report Mean Squared Error (MSE), Object Keypoint Similarity (OKS), and Probability of Detected Joints (PDJ@x), where  $x$  indicates correct keypoint detection if the keypoint lies within a distance of  $x \times d$ , with  $d$  being the diagonal of the bounding box containing the target. We evaluate the models on the APT36K Yang et al. (2022), APT10K Yu et al. (2021b), CrowdPose Li et al. (2019), and DeepLabCut Benchmark datasets Lauer et al. (2022), which include the TriMouse, Fish, and Marmoset datasets.

APT36k Dataset					APT10k Dataset				
Model	MSE	OKS	PDJ@0.08	PDJ@0.05	Model	MSE	OKS	PDJ@0.08	PDJ@0.05
TransPose	530.61	0.749	0.747	0.641	TransPose	732.52	0.548	0.621	0.492
YOLOv8-M	459.49	0.798	0.846	0.715	YOLOv8-M	423.89	0.567	0.643	0.544
YOLOv8-L	449.52	0.756	0.856	0.725	YOLOv8-L	<b>406.56</b>	0.567	0.656	0.516
ViPNAS	596.66	0.757	0.729	0.638	ViPNAS	647.12	0.503	0.671	0.503
ViTPose	490.20	0.804	0.916	<b>0.814</b>	ViTPose	548.07	0.562	<b>0.692</b>	<b>0.572</b>
Ours	<b>442.76</b>	<b>0.830</b>	<b>0.936</b>	0.799	Ours	482.69	<b>0.571</b>	0.682	0.565
Ours*	<b>404.37</b>	<b>0.832</b>	<b>0.946</b>	<b>0.804</b>	Ours*	<b>385.57</b>	<b>0.594</b>	<b>0.694</b>	<b>0.583</b>
TriMouse Dataset					Fish Dataset				
Model	MSE	OKS	PDJ@0.08	PDJ@0.05	Model	MSE	OKS	PDJ@0.08	PDJ@0.05
TransPose	119.15	0.885	0.925	0.886	TransPose	99.33	0.954	0.913	0.801
YOLOv8-M	82.34	0.901	0.912	0.86	YOLOv8-M	71.15	0.952	0.925	0.823
YOLOv8-L	<b>65.18</b>	0.899	0.928	<b>0.918</b>	YOLOv8-L	59.58	0.952	<b>0.943</b>	0.836
DeepLabCut	102.76	0.897	0.923	0.885	DeepLabCut	92.12	0.958	0.929	0.819
Ours	75.96	<b>0.904</b>	<b>0.946</b>	<b>0.916</b>	Ours	<b>54.24</b>	<b>0.959</b>	0.931	<b>0.842</b>
Ours*	<b>67.35</b>	<b>0.903</b>	<b>0.948</b>	0.915	Ours*	<b>47.59</b>	<b>0.960</b>	<b>0.962</b>	<b>0.838</b>
Marmoset Dataset					CrowdPose Dataset				
Model	MSE	OKS	PDJ@0.08	PDJ@0.05	Model	MSE	OKS	PDJ@0.08	PDJ@0.05
TransPose	223.64	0.734	0.796	0.714	RTMPose	<b>241.07</b>	0.715	<b>0.887</b>	<b>0.723</b>
YOLOv8-M	166.31	0.763	0.830	0.744	HRNet	371.41	0.653	0.763	0.625
YOLOv8-L	164.56	0.763	0.839	<b>0.792</b>	ViTPose	339.76	0.681	0.782	0.645
DeepLabCut	190.47	0.768	0.829	0.727	Ours	292.86	<b>0.734</b>	0.861	0.702
Ours	<b>161.95</b>	<b>0.779</b>	<b>0.859</b>	0.784	Ours*	<b>214.87</b>	<b>0.736</b>	<b>0.891</b>	<b>0.728</b>
Ours*	<b>159.68</b>	<b>0.784</b>	<b>0.858</b>	<b>0.799</b>					

through **four** Conv-Norm-ReLU layers. Outputs from both towers are concatenated and then further processed by a CNN with **four** Conv-Norm-ReLU layers. The final layer predicts the offset map  $\hat{K}_{om}^t$ . Note that we supervise GMSP Modules solely based on learning from the training frames within the video sequences. While processing subsequent test frames from the video, we freeze all weights associated with the GMSP Module.

- **BboxRegressor and Localizer Modules.** Localizers and bounding box regressors shown in Figure 1 have a similar architecture. The architectures are depicted in Figure 2 (b), (c), and (d). Initially, they first compute the attention map with their respective target model weights:  $w_{br}$ ,  $w_{loc}$ , and  $w_{kloc}$ , which is further processed with **three** Conv-Norm-ReLU layers. The box localizer  $\Lambda_L$  predicts localization of target with score map  $\hat{B}_{gm}$ , the keypoint localizer  $\Lambda_K$  predicts localization score maps of target keypoints  $\hat{K}_{gm}^t$ , and the Box Regressor  $\Lambda_B$  predicts dense LTRB offset maps of bounding box extent  $\hat{B}_{om}$ .

### 3.3 Training and Inference

This section outlines the steps involved in training the STEP framework, along with the associated loss functions. We then describe the inference procedure, including the confidence-based memory update, which ensures robust tracking and pose estimation within the STEP framework.

#### 3.3.1 Training

During the training phase, we randomly choose three frames from a video sequence comprising  $n$  frames denoted as  $\mathcal{S} = \{s_0, s_1, \dots, s_n\}$  annotated with bounding boxes and keypoints. Two frames are employed from this sampled set for training, leaving one for testing. For each training frame, we determine target state encodings as defined in Equation 4. The transformer module then predicts the target model weights, which are subsequently utilized by the regressor modules to perform localization, tracking, and keypoint estimation in the test frame. We train the Regressors in the following manner: the  $\Lambda_O(\cdot)$  predicts  $\hat{K}_{om}^t$ , the  $\Lambda_K(\cdot)$  predicts  $\hat{K}_{gm}^t$ , the  $\Lambda_B(\cdot)$  predicts  $\hat{B}_{om}$ , and the  $\Lambda_L(\cdot)$  predicts  $\hat{B}_{gm}$  for the test frame. The



**Table 2** Impact on metrics when initializing for target states using a pre-trained detector Zhang et al. (2022) versus ground-truth boxes.

Model	CrowdPose Dataset				
	Initialization	Per Frame Bounding Box	MSE	OKS	PDJ@0.08
<b>STEP</b>	Ground Truth	✗	292.86	0.734	0.861
<b>STEP*</b>	Ground Truth	✓	214.87	0.736	0.891
<b>STEP</b>	Detector	✗	292.31	0.731	0.835
<b>STEP*</b>	Detector	✓	213.62	0.733	0.854

**Table 3** Inference speed of our proposed approach compared to existing methods.

Model	Task	FPS	Per Frame Detector	$T_{100}$ (s)
<b>STEP</b>	Tracking + Pose Estimation	63	✗	1.63
<b>STEP*</b>	Pose Estimation	~63	✓	6.13
ViTPose Xu et al. (2022)	Pose Estimation	231	✓	4.97
TransPose Yang et al. (2021)	Pose Estimation	43	✓	6.87
YOLOv8-L Jocher et al. (2023)	Pose Estimation	113	✓	5.43
YOLOv8-M Jocher et al. (2023)	Pose Estimation	161	✓	5.16
RTM-Pose Jiang et al. (2023)	Pose Estimation	263	✓	4.92
DeeplabCut Lauer et al. (2022)	Pose Estimation	68	✓	6.01
HRNet Sun et al. (2019)	Pose Estimation	31	✓	7.77
ViPNAS Xu et al. (2021)	Pose Estimation	117	✓	5.40

respective ground truths for these predictions are  $K_{\text{gm}}^t$ ,  $K_{\text{om}}^t$ ,  $B_{\text{om}}$ , and  $B_{\text{gm}}$  obtained as discussed in Section 3.2. For  $B_{\text{gm}}$  and  $K_{\text{gm}}$ , we employ target classification as described in Bhat et al. (2019). We use a generalized Intersection over Union loss to predict  $B_{\text{om}}$ . Additionally, we apply mean-squared error loss to penalize the keypoint regression module for predicting  $K_{\text{om}}^t$ . Based on training-frame information, the GMSP Module is expected to effectively infer an enhanced target state of keypoints for the test frame. Therefore, we train the GMSP Module only on training frames to predict  $\hat{K}_{\text{gm}^{\text{sp}}}$  and freeze its weight while processing the test frame. It’s crucial to note that the loss applied to the regressors is derived explicitly from predictions made for the test frame, while the loss for the GMSP Module is based on predictions from the train frames. We now provide a detailed description of the loss functions for training in Section 3.3.2, which supervise the estimation of target-aware model localization weights  $w_{\text{loc}}$ ,  $w_{\text{kloc}}$  and offset map weights  $w_{\text{br}}$ ,  $w_{\text{kp}}$ , ensuring the end-to-end optimization of all learnable parameters in the model.

### 3.3.2 Loss Functions

We utilize the target classification loss, denoted as  $\mathcal{L}_{\text{cls}}$  similar to Bhat et al. (2019) for the Gaussian map predicted in the test frame through bounding box and keypoint regressors. The GMSP module is trained using the loss  $\mathcal{L}_{\text{cls}}$ , and this training is conducted on the training frames  $\mathcal{S}_{\text{train}}$  to predict

map  $\hat{K}_{\text{gm}^{\text{sp}}}$ , as opposed to the test frames. For the regression of offset maps associated with keypoints, we employ a hinged mean-squared loss denoted as  $\mathcal{L}_{\text{hom}}$ . This loss is only applied when the keypoint is visible in the annotated ground truth. We employ generalized Intersection over Union loss Rezatofighi et al. (2019) using LTRB bounding box representation for bounding box offset map regression. Loss functions employed during the training phase of STEP are defined in equation 7. In our experiments, we use  $\lambda_1 = \lambda_3 = \lambda_5 = 100$  and  $\lambda_2 = \lambda_4 = 10$ . To generate ground-truth offset maps for  $K_{\text{om}}$  and  $B_{\text{om}}$ , we use a stride value  $s = 16$  and Gaussian Maps  $B_{\text{gm}}$  and  $K_{\text{gm}}$  are generated at a spatial resolution of  $18 \times 18$ .

$$\begin{aligned} \mathcal{L}_{\text{test-frame}} = & \lambda_1 \mathcal{L}_{\text{cls}}(B_{\text{gm}}, \hat{B}_{\text{gm}}) + \lambda_2 \mathcal{L}_{\text{giou}}(B_{\text{om}}, \hat{B}_{\text{om}}) \\ & + \lambda_3 \mathcal{L}_{\text{cls}}(K_{\text{gm}}^t, \hat{K}_{\text{gm}}^t) + \lambda_4 \mathcal{L}_{\text{hom}}(K_{\text{om}}^t, \hat{K}_{\text{om}}^t) \end{aligned} \quad (5)$$

$$\mathcal{L}_{\text{train-frame}} = \mathcal{L}_{\text{gm}^{\text{sp}}} = \lambda_5 \mathcal{L}_{\text{cls}}(K_{\text{gm}}, \hat{K}_{\text{gm}^{\text{sp}}}) \quad (6)$$

$$\mathcal{L}_{\text{tot}} = \mathcal{L}_{\text{test-frame}} + \mathcal{L}_{\text{train-frame}} \quad (7)$$

### 3.3.3 Inference

During the inference phase, our approach requires initialization with a bounding box around the target object for the initial frame  $s_0 \in \mathcal{S}$  to establish target state information. This initialization could be done manually or with existing class-specific detectors. For the first frame, our training set is prepared by duplicating  $s_0$  such that  $\mathcal{S}_{\text{train}} = \{s_0, s_0\}$ .

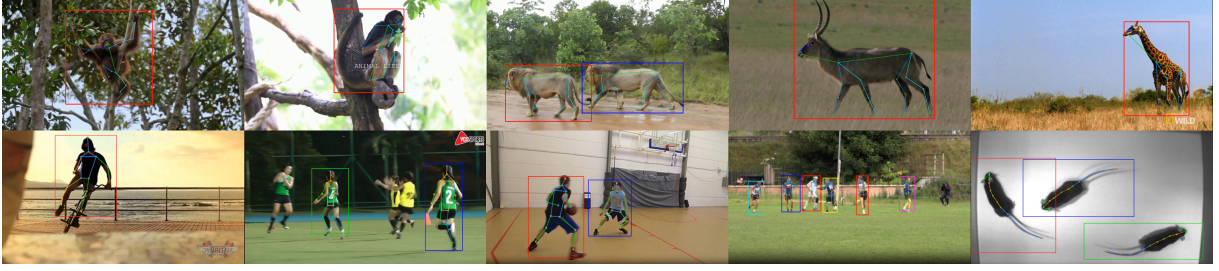


**Fig. 5** Frames from supplementary video on Animals [Yang et al. \(2022\)](#), Humans [Doering et al. \(2022\)](#), and Mouse [Lauer et al. \(2022\)](#) showcasing tracking and pose estimation. Please refer to the supplementary video for qualitative results on video sequences.

**Table 4** Training on Natural vs Synthetic sequences.

Model Trained On	Natural Sequences from APT36k			Synthetic Sequences from APT10k		
	MSE	OKS	PDJ@0.08	MSE	OKS	PDJ@0.08
Synthetic	374.28	0.635	0.749	395.76	0.764	0.818
Natural	356.68	0.733	0.872	397.98	0.791	0.861

Subsequently, our network predicts the sequence’s next frame  $s_1$  output. Following, this prediction  $s_1$  along with the predicted target state encodings, modifies our network’s memory for training, forming  $\mathcal{S}_{\text{train}} = \{s_0, s_1\}$ . We modify  $\mathcal{S}_{\text{train}}$  according to confidence thresholding, specifically when  $n$  key-points are predicted with confidence exceeding a certain threshold  $\tau_m$  in the map  $\hat{K}_{\text{gm}}^t$ . When there’s no memory update, the test frame is solely processed through the transformer, which is sufficient, enhancing performance speed. This is because the training frames and their corresponding target encodings remain unaltered. This iterative process continues until the end of the sequence. To determine the exact coordinates of keypoints and the bounding box in image space from the regressed offset maps  $\hat{K}_{\text{om}}^t$  and  $\hat{B}_{\text{om}}^t$ , we first extract the center location from the predicted confidence maps  $\hat{K}_{\text{gm}}^t$  and  $\hat{B}_{\text{gm}}^t$  by identifying the coordinate with the maximum value. We then query the offsets regressed at that location in  $\hat{K}_{\text{om}}^t$  and  $\hat{B}_{\text{om}}^t$ , map it back into the image space of  $s_i \in \mathbb{R}^{H_i \times W_i \times 3}$  by taking downsampling factor in Equation 2 into account and obtain keypoints and the bounding box.

**Implementation details.** We employ Adam optimizer with an initial learning rate set to  $10^{-4}$ , decayed by a factor of 0.1 after 50 epochs. We update the memory state of our network during inference when at least 50% of the total keypoints and the target localization both are predicted with

a confidence value greater than  $\tau_m = 0.6$ . All experiments were performed using NVIDIA GeForce RTX-4090 GPUs.

## 4 Results and Discussion

We assess our model across multiple datasets encompassing various species. APT36K [Yang et al. \(2022\)](#), consisting of 2,400 video clips collected and filtered from 30 animal species with 15 frames for each video, resulting in 36,000 frames in total for animal pose estimation and tracking, whereas APT10K [Yu et al. \(2021b\)](#) consists of 10,015 images collected and filtered from 23 animal families and 60 species. Our evaluation also spans across DeepLabCut Benchmark Datasets [DLC \(2021\)](#) [Lauer et al. \(2022\)](#) of diverse species in the lab setting, which includes the Tri-mouse dataset with 161 labeled frames where three wild-type male mice ran on a paper spool following odor trails; the Marmosets dataset with 7,600 labeled frames from 40 different marmosets collected from 3 different colonies, and Fish dataset with 100 labeled frames of Schools of inland silversides (*Menidia beryllina*). We utilized the CrowdPose [Li et al. \(2019\)](#) dataset, containing about 20,000 images and a total of 80,000 human poses with 14 labeled key points to assess the performance of STEP in human-based pose estimation and tracking.

**Table 5** Impact of the GMSP Module and  $\phi_{kp}$ .

Model Configuration	$\phi_{kp}$	Keypoint Initialization	APT36k Validation Split		
			MSE	OKS	PDJ@0.08
w GMSP	✓	✗	356.68	0.733	0.872
w/o GMSP	✓	✓	464.78	0.698	0.832
w GMSP	✗	✗	372.94	0.714	0.841
w/o GMSP	✗	✓	468.78	0.628	0.802

**Table 6** Impact of inclusion of embeddings in training features  $f_i$

$\phi_{loc}$	$\phi_{test}$	$X_{test}$	$\phi_{kp}$	MSE	OKS	PDJ@0.08
✓	✓	✓	✓	356.68	0.733	0.872
✗	✓	✓	✓	393.54	0.686	0.765
✓	✗	✓	✓	352.82	0.724	0.833
✗	✗	✓	✓	396.73	0.682	0.763
✓	✗	✗	✓	364.2	0.701	0.785

## 4.1 Data Processing

Our network is trained by sampling frames from sequences in datasets, as detailed in Section 3.3. We generate sequences from image-based datasets like APT10K and CrowdPose by applying random affine transformations during training. We create smooth transitions with random affine transformations for validation splits, resulting in 15-frame video sequences. These sequences are saved to evaluate the performance of existing methods. Figure 3 visually showcases qualitative tracking and pose estimation results on a sequence from the APT36k Dataset. The validation splits are formatted as  $(n_v, n_{tid}, n_f)$ , representing the number of video sequences, unique targets across all videos, and frames per video, respectively. Across the datasets— APT36k, APT0k, CrowdPose, Fish, TriMouse, and Marmoset— these splits contain  $(237, 348, 15)$ ,  $(201, 269, 15)$ ,  $(1572, 6803, 15)$ ,  $(24, 336, 15)$ ,  $(24, 78, 15)$ , and  $(199, 239, 15)$  data configurations, respectively. We train distinct models for each dataset to conduct both quantitative and qualitative evaluations. Since the different datasets utilize different keypoint landmarking systems, adjustments are necessary for the final layers of the Regressors in STEP. These minor modifications enable efficient fine-tuning and facilitate the model’s rapid adaptation to new datasets. However, we present results based on training each model from scratch for fair comparison. Our approach successfully learns to predict poses for different species within a dataset (e.g., APT36K, which includes 30 species) as they adhere to a consistent set of keypoint landmarks. All methods listed in Table 1 also follow a similar evaluation setup,

except for ViTPose. ViTPose employs joint training across all datasets to train a shared encoder and then employs dataset-specific decoders to regress keypoints.

## 4.2 Quantitative Evaluation.

In Table 1, we present a comparison of STEP with state-of-the-art methods on pose estimation in terms of Mean Squared Error (MSE), Object Keypoint Similarity (OKS), and Percentage of Detected Joints (PDJ).  $PDJ@x$  signifies a correct keypoint detection if it lies within the  $x \times d$  distance, where  $d$  is the diagonal of the bounding box containing the target. The top two performances are highlighted in bold. In **Ours**, we use only the initial frame’s bounding-box information and perform simultaneous tracking and pose estimation. In **Ours\***, we use per-frame ground-truth bounding box annotations to scale, crop, and center the images appropriately, similar to existing top-down approaches, to mitigate tracking errors and ensure a fair comparison of pose metrics. When evaluated using a top-down approach, our approach (Ours\*) outperforms existing state-of-the-art methods and demonstrates competitive performance in pose estimation while simultaneously performing the tracking task also (Ours), as shown in Table 1. Complementing the information in Table 1, Figure 4 displays the evaluation of Mean Squared Error (MSE) and Object Keypoint Similarity (OKS) scores for every individual keypoint. In Figure 8(b), a comparative assessment of tracking results is provided on the APT36K Dataset with existing tracking methods. The evaluation involves Intersection Over Union (IoU) and Overlap Precision (OP) of bounding boxes with thresholds ranging

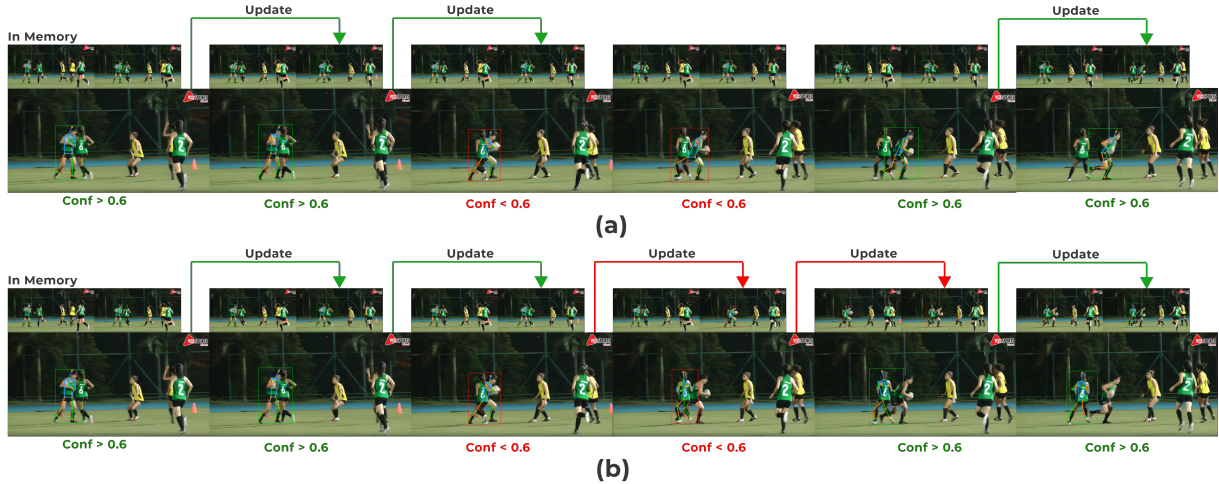


**Fig. 6** We demonstrate tracking and pose estimation during the occlusion of a target human instance by another human with a similar appearance. Zoom-in is recommended for clarity. Panel (a) illustrates memory updates occurring only when at least 50% of keypoints and the bounding box localization are predicted with a probability greater than  $\tau_m = 0.6$ . In contrast, panel (b) shows memory updates being performed regardless of the probability value. In both panels, frames with low confidence, which may introduce or propagate errors, are indicated by a red bounding box. In panel (b), STEP wrongly adjusts its confidence from the original target to the new instance based on the memory state. Subsequently, it starts tracking and performing pose estimation on the new object.

**Table 7** Impact of the number of training frames used,  $|\mathcal{S}_{\text{train}}|$ .

#Training frames	APT36k (Val Split)		APT10k (Val Split)	
	MSE	OKS	MSE	OKS
1 initial	465.48	0.697	536.69	0.684
1 initial + 1 recent	360.87	0.723	397.30	0.768
1 initial + 2 recent	358.31	0.723	395.82	0.778
Rolling recent-2	495.89	0.682	543.49	0.673
Rolling recent-3	492.62	0.674	538.95	0.686
Conf. Rolling-2	356.68	0.733	395.76	0.764
Conf. Rolling-3	357.38	0.742	394.89	0.764

from  $(0, 1]$  between STEP and existing tracking methods.

#### 4.2.1 Automatic Initialization

Our proposed approach requires initialization with a bounding box to establish information on the target of interest. We conduct an experiment to assess the effect of initialization by employing a pre-trained Detector [Zhang et al. \(2022\)](#) to identify humans in the validation split of the CrowdPose Dataset [Li et al. \(2019\)](#). The detector provides class-specific bounding boxes, and since CrowdPose is a human dataset, we filter out the predicted bounding boxes specific to the person category. However, the detector can sometimes mistakenly identify non-person objects as human or detect instances whose corresponding keypoint annotations are unavailable in the ground truth, which

can hinder metric evaluation. To address this, we filter the predicted bounding boxes by selecting those with the maximum Intersection over Union (IoU) with the annotated boxes in the dataset. We run STEP on validation splits with initializations from the detector and with annotation available in the CrowdPose dataset and observe the minimal impact on metrics, as evident from Table 2. Initializing STEP with a pre-trained detector [Zhang et al. \(2022\)](#) has minimal impact on performance while fully automating the process.

#### 4.3 Qualitative Results

A supplementary video is available, demonstrating the results on video sequences of animals from [Yang et al. \(2022\)](#), humans from [Doering et al. \(2022\)](#), and mice and fishes from [Lauer et al. \(2022\)](#).



We present a frame from the sequences in the supplementary video in Figure 5.

#### 4.4 Inference Speed Analysis

For inference speed, We evaluate all methods on an equivalent number of frames from the respective datasets, matching the number of frames in the validation split of APT-36K, as shown in Table 3. Given the differences in evaluation settings for pose estimation across SOTA methods, we established the following protocols to asses comparison: we fix the resolution of all frames to ( $H \times W = 256 \times W$ ) maintaining the aspect ratio for STEP (Ours). For Deeplabcut and STEP\* (Ours\*), we cropped detected instances into square patches and resized them to ( $256 \times 256$ ). For the other methods listed in Table 1, we employed cropping similar to that used in ViTPose, i.e., more horizontal cropping for animals ( $192 \times 256$ ) and more vertical cropping for humans ( $256 \times 192$ ). Note that our proposed method, STEP, achieves an average speed of 63 FPS for both tracking and pose estimation tasks while requiring initialization for the first-most frame only. In contrast, STEP\* and other top-down approaches face a performance bottleneck of per-frame detections. For object detection, we employ well-established detectors, specifically MegaDetector Hernandez et al. (2024) for animal detection and Dino Zhang et al. (2022) for human detection, achieving inference speeds of 29 FPS and 22 FPS, respectively. In Table 3, We include  $T_{100}$  to clearly demonstrate the total time required to process 100 frames when both tasks are performed sequentially with Dino Detector, facilitating a more straightforward assessment. Furthermore, we would like to highlight that both STEP and STEP\* maintain tracking information across videos. In contrast, other methods necessitate an additional step to establish target correspondence across frames, such as tracklet stitching in DeepLabCut with an FPS of 2400 Lauer et al. (2022). FPS evaluations were conducted with a batch size of 1, and all experiments were performed on a device equipped with an NVIDIA Geforce RTX-4090.

The video also contains results using the top-down approach with STEP\*, utilizing per-frame bounding box information. Since the detections for each frame are known in advance, STEP\* can manage newly entered objects, maintain tracking, and estimate their respective poses.

#### 4.5 A Case Study on AMC Live Streams

Utilizing STEP, we extracted self-motion and pose information from live video streams at the Awajishima Monkey Center (AMC) in Hyogo prefecture, Japan (Video recordings used with permission, Live Stream: [Link](#)). The center accommodates a large group of freely moving macaque monkeys, capturing their behavior through a live camera overlooking a popular visitor area. While macaque activity is extensively studied in animal ethology, typically at a coarse temporal scale, focusing on proportions of time spent on various activities like foraging and grooming Jaman and Huffman (2013), our emphasis was on a finer measurement of self-motion. We aimed to leverage STEP to understand alterations in monkey behavior throughout the day and in response to events such as feeding. Observations reveal that monkeys generally move at median speeds below 1 m/sec (Figure 7(a)), but they can also exhibit rapid movements (Figure 7(b)). Elevated activity is noticeable during feeding episodes, as depicted in Figure 7(c). Figure 8(a) illustrates the movement speed observed across different track-ids on streams over two days. It’s important to note that the analysis is confined to 2D-image space, excluding consideration of the third dimension. We employed an existing detector Lyu et al. (2022) (fine-tuned on monkeys) to initialize the STEP tracking and estimate the pose for subsequent frames. STEP demonstrates satisfactory performance, effectively quantifying behavioral changes in a setting with high variability in animal occupancy, scale, and pose.

#### 4.6 Ablation Study

We conducted multiple ablation studies to assess the performance of the proposed STEP approach, utilizing the APT36k and APT10k datasets. The reported metrics showcase the results obtained when all variants were trained for 100 epochs and subsequently evaluated on a reduced validation split consisting of 150 video sequences from each dataset.



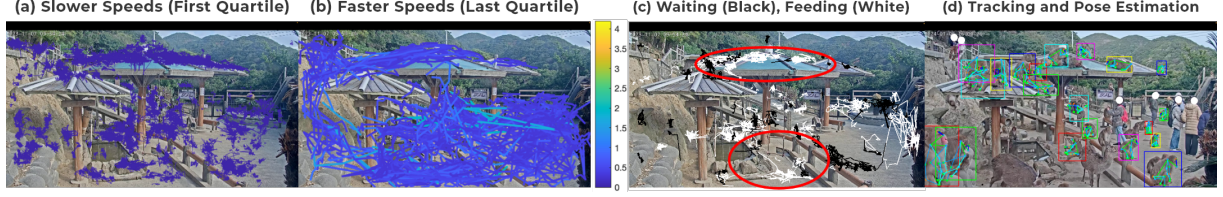


**Fig. 7** (a) slowest and (b) fastest quartiles of self-movement velocities over recordings from 2 days. The provision of feeding results in animals moving towards food, causing movement from black to white clusters, illustrated in (c). Trajectories are plotted by tracking the center of the bounding box across all selected tracks. A high occupancy representative scene with overlaid tracks and poses is shown in (d).<sup>†</sup>

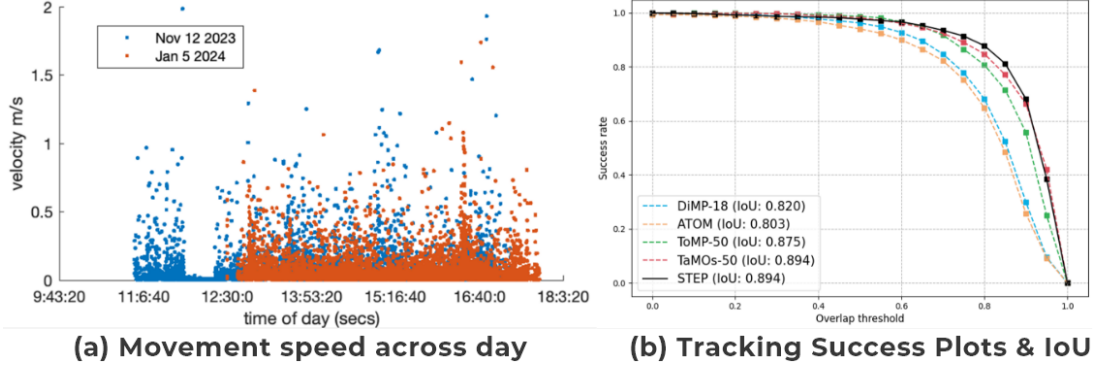


**Fig. 8** (a) Movement velocity observed overall recorded data from AMC (tracks longer than 1 sec). Increased movement typically aligns with feeding episodes. Distances are derived from AMC’s perspective on Google Maps. (b) IoU and Overlap Precision ( $OP_T$ ) for bounding box tracking in STEP compared with existing methods: DiMP [Bhat et al. \(2019\)](#), ToMP [Mayer et al. \(2022\)](#), ATOM [Danelljan et al. \(2019\)](#), and TAMOS [Mayer et al. \(2024\)](#).

#### 4.6.1 Natural vs Synthetic Data sequence.

Table 4 presents metrics illustrating the impact on performance when training the model on natural and synthetic sequences. The model effectively generalizes natural video sequences even when trained on synthetic sequences.

#### 4.6.2 Architectural Ablations

In Table 5, we examine the influence of the GMSP module. We hypothesize that the GMSP module learns soft predictions for the keypoints. To validate this, we experimented by removing the GMSP module and replacing it with ground-truth keypoints. In this configuration, we omitted the branch injecting features from GMSP to regression modules for test frames. This setup resulted in a decrease in overall performance. The inclusion of the GMSP module not only eliminates the need for keypoint initialization but also contributes to increased performance. Additionally,

the soft predictions generated by GMSP provide more enriched information for keypoint encodings than the keypoint initialization setting. The incorporation of  $\phi_{loc}$  has been demonstrated to improve performance, as indicated in [Mayer et al. \(2022\)](#). Similarly, we explore the impact of including  $\phi_{kp}$  in determining target state encodings. As presented in Table 5, a notable performance enhancement in pose estimation is attributed to incorporating the learnable embedding for each keypoint. Furthermore, in Table 6, we provide a more detailed assessment of the impact of test-frame embedding  $\phi_{test}$ , bounding box embedding  $\phi_{loc}$  and on the inclusion of test-frame  $X_{test}$  for model weight prediction.

#### 4.6.3 Memory Update

In Table 7, we examine the impact of the number of training frames for target model weight predictions during inference. By updating training frames  $\mathcal{S}_{train}$  using confidence thresholding  $\tau_m$  as detailed

in Section 3.3, we observe a performance improvement. In Figure 6, we demonstrate the robustness of memory update for accurate tracking and pose estimation of target objects.

#### 4.7 Limitations

Our proposed approach requires initialization through a bounding box for the first-most frame in a given video to infer target state encodings. This initialization establishes the target of interest and could be manual or fully automated using object detectors such as Lyu et al. (2022) Zhang et al. (2022). We observed that the network tends to estimate the pose keypoints within the predicted bounding box or, conversely, predicts a bounding box that encompasses the predicted keypoints. As our approach operates simultaneously, errors originating from one task can negatively impact the accuracy of the other task. This is evident from the metrics evaluated between "Ours" and "Ours\*" in Table 1.

### 5 Conclusion

This work proposes a novel framework for Simultaneous Tracking and Estimation of Pose across diverse animal species and humans. Our method estimates the pose of the object of interest while simultaneously tracking it, utilizing a Transformer-based discriminative target model prediction approach. The key contributions of our framework include the Gaussian Soft Map Prediction module and the Offset Map Regression Adapter module, which effectively removes the dependency on keypoint initialization to estimate target state encodings. We show that the network equipped with the proposed modules performs better than the version relying on keypoint initialization. Unlike traditional top-down approaches that depend on per-frame detections for pose estimation and are thus limited by speed bottlenecks, our method overcomes this issue by relying on efficient tracking. The proposed STEP framework achieves state-of-the-art performance in both tracking and pose estimation tasks. Lastly, we showcase the robustness of our approach in challenging video scenarios with high animal occupancy, underscoring its effectiveness in both tracking and pose estimation.

### References

- Ai Y, Qi Y, Wang B, et al (2024) Domain-adaptive 2d human pose estimation via dual teachers in extremely low-light conditions. In: European Conference on Computer Vision, Springer, pp 221–239
- Bhat G, Danelljan M, Gool LV, et al (2019) Learning discriminative model prediction for tracking. In: Proceedings of the IEEE/CVF international conference on computer vision, pp 6182–6191
- Bouchrika I, Goffredo M, Carter J, et al (2011) On using gait in forensic biometrics. *Journal of forensic sciences* 56(4):882–889
- Carion N, Massa F, Synnaeve G, et al (2020) End-to-end object detection with transformers. In: European conference on computer vision, Springer, pp 213–229
- Chen X, Yan B, Zhu J, et al (2021) Transformer tracking. In: Proceedings of the IEEE/CVF conference on computer vision and pattern recognition, pp 8126–8135
- Coria-Avila GA, Pfaus JG, Orihuela A, et al (2022) The neurobiology of behavior and its applicability for animal welfare: A review. *Animals* 12(7):928
- Dai K, Wang D, Lu H, et al (2019) Visual tracking via adaptive spatially-regularized correlation filters. In: Proceedings of the IEEE/CVF Conference on Computer Vision and Pattern Recognition, pp 4670–4679
- Danelljan M, Bhat G, Khan FS, et al (2019) Atom: Accurate tracking by overlap maximization. In: Proceedings of the IEEE/CVF conference on computer vision and pattern recognition, pp 4660–4669
- Deng J, Dong W, Socher R, et al (2009) Imagenet: A large-scale hierarchical image database. In: 2009 IEEE conference on computer vision and pattern recognition, Ieee, pp 248–255
- DLC (2021) DeepLabCut Benchmark Datasets — benchmark.deeplabcut.org. <https://benchmark.deeplabcut.org/datasets.html>

- Doering A, Chen D, Zhang S, et al (2022) Pose-track21: A dataset for person search, multi-object tracking and multi-person pose tracking. In: Proceedings of the IEEE/CVF Conference on Computer Vision and Pattern Recognition, pp 20963–20972
- Dosovitskiy A, Beyer L, Kolesnikov A, et al (2020) Transformers for image recognition at scale. arXiv preprint arXiv:2010.11929
- Duan K, Bai S, Xie L, et al (2019) Center-net: Keypoint triplets for object detection. In: Proceedings of the IEEE/CVF international conference on computer vision, pp 6569–6578
- Ge Z, Liu S, Wang F, et al (2021) YoloX: Exceeding yolo series in 2021. arXiv preprint arXiv:2107.08430
- Hernandez A, Miao Z, Vargas L, et al (2024) Pytorch-wildlife: A collaborative deep learning framework for conservation. [arXiv:2405.12930](https://arxiv.org/abs/2405.12930)
- Insafutdinov E, Pishchulin L, Andres B, et al (2016) Deeppercut: A deeper, stronger, and faster multi-person pose estimation model. In: Computer Vision—ECCV 2016: 14th European Conference, Amsterdam, The Netherlands, October 11–14, 2016, Proceedings, Part VI 14, Springer, pp 34–50
- Jaman MF, Huffman MA (2013) The effect of urban and rural habitats and resource type on activity budgets of commensal rhesus macaques (*macaca mulatta*) in bangladesh. *Primates* 54:49–59
- Jiang P, Ergu D, Liu F, et al (2022) A review of yolo algorithm developments. *Procedia Computer Science* 199:1066–1073
- Jiang T, Lu P, Zhang L, et al (2023) Rtmpose: Real-time multi-person pose estimation based on mmpose. <https://doi.org/10.48550/ARXIV.2303.07399>, URL <https://arxiv.org/abs/2303.07399>
- Jocher G, Chaurasia A, Qiu J (2023) Yolo by ultralytics
- Lauer J, Zhou M, Ye S, et al (2022) Multi-animal pose estimation, identification and tracking with deeplabcut. *Nature Methods* 19(4):496–504
- Li B, Wu W, Wang Q, et al (2018) Evolution of siamese visual tracking with very deep networks. arxiv 2018. arXiv preprint arXiv:1812.11703
- Li C, Lee GH (2023) Scarcenet: Animal pose estimation with scarce annotations. In: Proceedings of the IEEE/CVF Conference on Computer Vision and Pattern Recognition, pp 17174–17183
- Li J, Wang C, Zhu H, et al (2019) Crowdpose: Efficient crowded scenes pose estimation and a new benchmark. In: Proceedings of the IEEE/CVF conference on computer vision and pattern recognition, pp 10863–10872
- Li K, Wang S, Zhang X, et al (2021a) Pose recognition with cascade transformers. In: Proceedings of the IEEE/CVF conference on computer vision and pattern recognition, pp 1944–1953
- Li R, Li Q, Yang S, et al (2024) An efficient and accurate 2d human pose estimation method using vttranspose network. *Scientific Reports* 14(1):7608
- Li Y, Zhang S, Wang Z, et al (2021b) Tokenpose: Learning keypoint tokens for human pose estimation. In: Proceedings of the IEEE/CVF International conference on computer vision, pp 11313–11322
- Li Y, Mao H, Girshick R, et al (2022) Exploring plain vision transformer backbones for object detection. In: European Conference on Computer Vision, Springer, pp 280–296
- Lyu C, Zhang W, Huang H, et al (2022) Rtmddet: An empirical study of designing real-time object detectors. arXiv preprint arXiv:2212.07784
- Mathis A, Mamidanna P, Cury KM, et al (2018) Deeplabcut: markerless pose estimation of user-defined body parts with deep learning. *Nature neuroscience* 21(9):1281–1289
- Mayer C, Danelljan M, Bhat G, et al (2022) Transforming model prediction for tracking. In: Proceedings of the IEEE/CVF conference on

- computer vision and pattern recognition, pp 8731–8740
- Mayer C, Danelljan M, Yang MH, et al (2024) Beyond sot: Tracking multiple generic objects at once. In: Proceedings of the IEEE/CVF Winter Conference on Applications of Computer Vision, pp 6826–6836
- Pereira TD, Tabris N, Matsliah A, et al (2022) Slep: A deep learning system for multi-animal pose tracking. *Nature methods* 19(4):486–495
- Pishchulin L, Insafutdinov E, Tang S, et al (2016) Deepcut: Joint subset partition and labeling for multi person pose estimation. In: Proceedings of the IEEE conference on computer vision and pattern recognition, pp 4929–4937
- Rezatofighi H, Tsoi N, Gwak J, et al (2019) Generalized intersection over union: A metric and a loss for bounding box regression. In: Proceedings of the IEEE/CVF conference on computer vision and pattern recognition, pp 658–666
- Strudel R, Garcia R, Laptev I, et al (2021) Segmenter: Transformer for semantic segmentation. In: Proceedings of the IEEE/CVF international conference on computer vision, pp 7262–7272
- Sun JJ, Ryou S, Goldshmid RH, et al (2022) Self-supervised keypoint discovery in behavioral videos. In: Proceedings of the IEEE/CVF Conference on Computer Vision and Pattern Recognition, pp 2171–2180
- Sun K, Xiao B, Liu D, et al (2019) Deep high-resolution representation learning for human pose estimation. In: Proceedings of the IEEE/CVF conference on computer vision and pattern recognition, pp 5693–5703
- Toshev A, Szegedy C (2014) Deeppose: Human pose estimation via deep neural networks. In: Proceedings of the IEEE conference on computer vision and pattern recognition, pp 1653–1660
- Vaswani A, Shazeer N, Parmar N, et al (2017) Attention is all you need. *Advances in neural information processing systems* 30
- Wang N, Zhou W, Wang J, et al (2021) Transformer meets tracker: Exploiting temporal context for robust visual tracking. In: Proceedings of the IEEE/CVF conference on computer vision and pattern recognition, pp 1571–1580
- Wei SE, Ramakrishna V, Kanade T, et al (2016) Convolutional pose machines. In: Proceedings of the IEEE conference on Computer Vision and Pattern Recognition, pp 4724–4732
- Welch G, Bishop G, et al (1995) An introduction to the kalman filter. Chapel Hill, NC, USA
- Xiao B, Wu H, Wei Y (2018) Simple baselines for human pose estimation and tracking. In: Proceedings of the European conference on computer vision (ECCV), pp 466–481
- Xu L, Guan Y, Jin S, et al (2021) Vipnas: Efficient video pose estimation via neural architecture search. In: Proceedings of the IEEE/CVF Conference on Computer Vision and Pattern Recognition, pp 16072–16081
- Xu Y, Wang Z, Li Z, et al (2020) Siamfc++: Towards robust and accurate visual tracking with target estimation guidelines. In: Proceedings of the AAAI conference on artificial intelligence, pp 12549–12556
- Xu Y, Zhang J, Zhang Q, et al (2022) Vitpose: Simple vision transformer baselines for human pose estimation. *Advances in Neural Information Processing Systems* 35:38571–38584
- Yan B, Peng H, Fu J, et al (2021) Learning spatio-temporal transformer for visual tracking. In: Proceedings of the IEEE/CVF international conference on computer vision, pp 10448–10457
- Yang S, Quan Z, Nie M, et al (2021) Transpose: Keypoint localization via transformer. In: Proceedings of the IEEE/CVF International Conference on Computer Vision, pp 11802–11812
- Yang Y, Yang J, Xu Y, et al (2022) Apt-36k: A large-scale benchmark for animal pose estimation and tracking. *Advances in Neural Information Processing Systems* 35:17301–17313

- Ye S, Zhang Y, Hu J, et al (2023) Distilpose: Tokenized pose regression with heatmap distillation. In: Proceedings of the IEEE/CVF Conference on Computer Vision and Pattern Recognition, pp 2163–2172
- Yu B, Tang M, Zheng L, et al (2021a) High-performance discriminative tracking with transformers. In: Proceedings of the IEEE/CVF International Conference on Computer Vision, pp 9856–9865
- Yu H, Xu Y, Zhang J, et al (2021b) Ap-10k: A benchmark for animal pose estimation in the wild. arXiv preprint arXiv:210812617
- Yuan Y, Fu R, Huang L, et al (2021) Hrformer: High-resolution vision transformer for dense predict. Advances in Neural Information Processing Systems 34:7281–7293
- Zhang H, Li F, Liu S, et al (2022) Dino: Detr with improved denoising anchor boxes for end-to-end object detection. arXiv preprint arXiv:220303605
- Zhang Z, Zhong B, Zhang S, et al (2021) Distractor-aware fast tracking via dynamic convolutions and mot philosophy. In: Proceedings of the IEEE/CVF conference on computer vision and pattern recognition, pp 1024–1033
- Zheng L, Tang M, Chen Y, et al (2020) Learning feature embeddings for discriminant model based tracking. In: Computer Vision–ECCV 2020: 16th European Conference, Glasgow, UK, August 23–28, 2020, Proceedings, Part XV 16, Springer, pp 759–775